

Planetesimals on eccentric orbits erode rapidly

LUKAS CEDENBLAD,^{1,2} NOEMI SCHAFER,³ ANDERS JOHANSEN,^{3,4} B. MEHLIG,⁵ AND DHRUBADITYA MITRA¹ 

¹*NORDITA, Royal Institute of Technology and Stockholm University, Roslagstullsbacken 23, SE-10691 Stockholm, Sweden*

²*Department of Physics, AlbaNova University Center, Stockholm University, SE-10691 Stockholm, Sweden.*

³*Lund Observatory, Department of Astronomy and Theoretical Physics, Lund University, Box 43, 22100 Lund, Sweden.*

⁴*Centre for Star and Planet Formation, Globe Institute, University of Copenhagen, Oster Voldgade 5–7, 1350 Copenhagen, Denmark*

⁵*Department of Physics, Gothenburg University, SE-41296 Gothenburg, Sweden*

ABSTRACT

We investigate the possibility of erosion of planetesimals in a protoplanetary disk. We use theory and direct numerical simulations (Lattice Boltzmann Method) to calculate the erosion of large – much larger than the mean-free-path of gas molecules – bodies of different shapes in flows. We find that erosion follows a universal power-law in time, at intermediate times, independent of the Reynolds number of the flow and the initial shape of the body. Consequently, we estimate that planetesimals in eccentric orbits, of even very small eccentricity, rapidly (in about hundred years) erodes away if the semi-major axis of their orbit lies in the inner disk – less than about 10 au. Even planetesimals in circular orbits erode away in approximately ten thousand years if the semi-major axis of their orbits are $\lesssim 0.6$ au.

1. INTRODUCTION

According to our present understanding, the process of formation of planets begins with the growth of micrometer sized dust in a protoplanetary disk (Armitage 2010). Dust particles move around the central star in Keplerian orbits and at the same time settle down to the midplane of the disk. Let us assume that whenever two dust particles collide, they stick together. Consider an aggregate of dust particles – a planetesimal – rotating around the central star. The planetesimal rotates with Keplerian speed while the gas around it rotates at a slightly sub-Keplerian speed. Hence, the planetesimal feels a *headwind* thereby loses angular momentum due to drag forces and spirals into the star very rapidly in about a few hundred years. Within this time the planetesimal is estimated to at most grow to the size of few meters (Youdin 2010; Armitage 2010). This *meter-sized barrier* appears to prevent planet formation. Over the years, several possible solutions, including the streaming instability (Youdin & Goodman 2005; Johansen et al. 2007), concentration in vortices and pressure bumps (Barge & Sommeria 1995; Klahr & Bodenheimer 2006; Johansen et al. 2009) enhanced rate of collision due to turbulence (Mitra et al. 2013), gravitational collapse of clouds of pebbles (Klahr & Schreiber 2020, 2021), to name a few, have been suggested, see also

Johansen et al. (2014), for a review. To make matters worse, it is quite unlikely that whenever two dust particles collide they stick. Possible outcomes of collisions could be sticking, complete or partial, fragmentation, or bouncing depending on the mechanical, e.g., relative velocities on collision, and thermodynamic (e.g., ambient temperature) conditions (Wilkinson et al. 2008; Blum & Wurm 2008; Wettlaufer 2010; Zsom et al. 2011). The dust aggregate that forms in this manner is likely to be very loosely bound, therefore could it not break up? There are several possibilities, e.g., : (a) two dust aggregates may collide and fragment and (b) the gas can erode the dust aggregate away. In this paper, we investigate the second possibility which has received considerable attention recently (Paraskov et al. 2006; Musiolik et al. 2018; Demirci et al. 2019; Kruss et al. 2020; Schaffer et al. 2020; Rozner et al. 2020; Demirci et al. 2020).

The rest of the paper is organized in the following manner. We first consider the mathematical problem of erosion of a solid by a fluid. In section 2 we describe our model in terms of several dimensionless parameters and next, following Ristroph et al. (2012); Moore et al. (2013) and Mac Huang et al. (2015), present a theoretical framework to understand this problem. In section 3 we show the results of our numerical simulation of erosion using the Lattice Boltzmann Method (LBM). In particular, we demonstrate that if the stress holding the body is small enough, the solid erodes away in a finite time. In section 3.2 we show the relevance of these

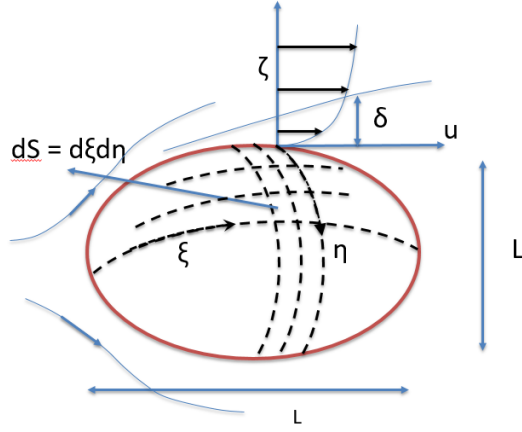


Figure 1. A sketch of a boulder of length scale L with a flow around it. Far away from the body the velocity of the flow is \mathbf{U} . We use a set of a generalized coordinate system ξ, η, ζ such that ξ – η form a set of surface coordinates and ζ is the coordinate perpendicular to the surface. An infinitesimal surface area $dS = d\xi d\eta$. Ahead of the body is a point in the flow where the velocity is zero relative to the boulder. This point is called the stagnation point. We choose ξ such that all the points with a constant ξ are equidistant from the stagnation point and as ξ increases we move away from the stagnation point. The flow velocity is zero at the surface of the boulder – no-slip boundary condition. The tangential component of velocity u rises sharply from zero to its free-stream value $|\mathbf{U}|$ within a small distance δ , the thickness of the boundary layer. In the coordinate system chosen δ is a function of ξ alone.

results for planetesimals in protoplanetary disks. We conclude in section 4.

2. MODEL

We consider a large boulder with a characteristic length scale L moving with a speed U in a fluid with dynamic viscosity $\mu = \rho\nu$, where ρ is its density and ν its kinematic viscosity. We assume that the Reynolds number, $\text{Re} \equiv UL/\nu$, of the flow is large, but the flow is not otherwise turbulent. Let us consider this problem in a frame fixed with the boulder. In this frame the speed of the flow far away from the boulder is U . We consider the following model of erosion (Jäger et al. 2017; Schaffer et al. 2020) : the rate of mass-loss from an infinitesimal surface area dS of the body is given by

$$\dot{m}dS = \begin{cases} \kappa_{\text{er}} (\tau_f - \tau_s) dS, & \text{for } \tau_f > \tau_s \\ 0, & \text{otherwise.} \end{cases} \quad (1)$$

Here, τ_f is the normal component of the shear stress due to the fluid, τ_s is a threshold stress – the solid starts eroding once the fluid stress exceeds this threshold stress – and κ_{er} is a constant of proportionality. Equation 1

is purely empirical. It is often used in estimations of erosion of river beds (Shields 1936; Subhasish 2014). However, if we assume that the erosion rate is an analytic function of $\tau \equiv \tau_f - \tau_s$, then for small τ Eq. (1) holds. Both the erosion coefficient, κ_{er} , and the threshold stress, τ_s depend on the material properties of the solid, e.g., its composition and porosity. Note that in Eq. (1) m has the dimension of mass/area and κ_{er} has the dimension of inverse velocity. Let us choose a set of generalized coordinates ξ, η, ζ such that ξ – η form a set of surface coordinate and ζ is the coordinate perpendicular to the surface, see Fig. (1). The fluid stress $\tau_f \equiv \mu \partial u / \partial \zeta$ where u is the component of the flow velocity along the tangential direction. If the fluid stress is larger than the solid stress, the boulder starts eroding. We also assume that the erosion proceeds on a characteristic time scale much slower than $T \equiv L/U$. As the body erodes, the flow around the body changes, this in turn changes the fluid stress and hence the rate of erosion. This is an example of a free boundary problem. Ahead of the body is a point in the flow whose velocity is zero relative to the boulder. This point is called the stagnation point. We choose ξ such that all the points with a constant ξ are equidistant from the stagnation point and as ξ increases we move away from the stagnation point¹. The flow velocity is zero at the surface of the boulder – no-slip boundary condition. The tangential component of velocity, u , rises sharply from zero to its free-stream value U within a small distance δ , the thickness of the boundary layer. The theory of laminar boundary layer (see, e.g., Landau & Lifshitz 1959, chapter IV) estimates δ as

$$\delta = \sqrt{\frac{\nu \xi}{U}}, \quad (2)$$

valid for ξ not too close to zero, i.e., away from the stagnation point. This allows us to estimate the fluid stress as

$$\tau_f \sim \mu \frac{U}{\delta}. \quad (3)$$

2.1. Dimensionless numbers

We use L as our characteristic length scale and U as our characteristic velocity scale to obtain $T \equiv L/U$ as our characteristic timescale. We define the erosion number to be $\text{Er} \equiv \kappa_{\text{er}} U$. If the typical fluid stress is larger

¹ For example, if the boulder is a sphere of radius L we choose a spherical polar coordinate systems with the z -axis pointing along the flow. Then, $d\xi = L d\theta$ and $d\eta = L \sin(\theta) d\phi$, and $dS = L^2 \sin(\theta) d\theta d\phi$ where θ is the polar angle and ϕ the azimuthal angle, respectively. Lines of constant ξ are the latitudes of this sphere and the lines of constant η the longitudes. The stagnation point lies outside the sphere somewhere on the z -axis.

than the critical solid stress, we expect erosion. We define a corresponding dimensionless number, the threshold number (Th)

$$\text{Th} \equiv \frac{\tau_f}{\tau_s}. \quad (4)$$

Erosion happens only if $\text{Th} > 1$. The three dimensionless numbers that completely specify our problem are: the Reynolds number ($\text{Re} \equiv UL/\nu$), the erosion number (Er) and the dimensionless threshold (Th). To obtain a typical value for the Erosion number and the dimensionless threshold, we need to estimate a typical value for the fluid stress. We use two different estimates for the thickness of the boundary layer, and consequently two different estimates for the fluid stress:

$$\delta_{\max} = \sqrt{\frac{\nu L}{U}} \quad \delta_{\text{typ}} = \sqrt{\frac{\nu \Lambda^2 \lambda}{U}} \quad (5a)$$

$$\tau_f^{\min} = \frac{\rho U^2}{\sqrt{\text{Re}}} \quad \tau_f^{\text{typ}} = \frac{\rho U^2}{\Lambda \sqrt{\text{Ma}}} \quad (5b)$$

$$\text{Th}_{\min} = \frac{1}{\sqrt{\text{Re}}} \frac{\rho U^2}{\tau_s} \quad \text{Th}_{\text{typ}} = \frac{1}{\Lambda \sqrt{\text{Ma}}} \frac{\rho U^2}{\tau_s} \quad (5c)$$

In the left column of (5), we have used the length of the eroding body L as the length scale that determines the maximum value of the boundary layer thickness which corresponds to minimum value of the fluid stress. In the right column, to estimate the typical value of the fluid stress we use a length scale that is Λ^2 times the mean-free-path λ , where Λ^2 , the inverse Knudsen number, is large – about 100. We also use $\nu \sim c_s \lambda$ where c_s is the speed of sound – a familiar result from the kinetic theory of gases (see, e.g., Lifshitz & Pitaevskii 1993).

2.2. Theoretical framework

Recently, a collection of remarkable papers (Ristroph et al. 2012; Moore et al. 2013; Mac Huang et al. 2015) studied erosion of bodies in fluid flows both analytically and experimentally. For the sake of completeness we summarize their arguments below.

First, assume that τ_s is so small that it can be safely ignored. We can then estimate the rate of total mass loss as

$$\frac{dM}{dt} \approx -\kappa_{\text{er}} \int \frac{\mu U}{\delta} d\xi d\eta = -\kappa_{\text{er}} \frac{\mu U^{3/2}}{\sqrt{\nu}} \int \frac{d\xi d\eta}{\sqrt{\xi}} \quad (6)$$

$$= -\rho_g \kappa_{\text{er}} \sqrt{U^3 \nu} L^{3/2}. \quad (7)$$

Here, $M(t)$ is the total mass of the body. Next, assume the material density of the body to be a constant, ρ_\bullet . Then, Eq. (7) can be written as a differential equation for the instantaneous volume $V(t)$,

$$\frac{dV}{dt} = -C \kappa_{\text{er}} \left(\frac{\rho_g}{\rho_\bullet} \right) \sqrt{U^3 \nu} \sqrt{V}. \quad (8)$$

We integrate this differential equation, with the initial condition that at $t = 0$ the volume was V_0 , to obtain

$$\frac{V}{V_0} = \left(1 - \frac{t}{t_*} \right)^2, \quad (9)$$

with

$$\frac{t_*}{T} = \left(\frac{\rho_\bullet}{\rho_g} \right) \frac{1}{C \text{Er}} \sqrt{\text{Re}}, \quad (10)$$

where $L_0 \equiv V_0^{1/3}$, and $\text{Re} \equiv UL_0/\nu$ is the Reynolds number of the body at its initial size. Given an initial volume, V_0 , the characteristic time by which it erodes away is t_* given in Eq. (10). The constant C is a constant that depends on the shape of the body.

It is important to emphasize here that this theory shows that the process of erosion is a power-law in time; hence, we cannot meaningfully define a characteristic time scale of erosion or a rate of erosion. The only meaningful time scale is the time scale t_* .

Several simplifying assumptions made above must now be qualified. First, the expression for the boundary layer is for a laminar boundary layer, strictly speaking, valid for small Reynolds number and also if the body is not too large. As the Reynolds number of the flow increases, the boundary layer separates (Landau & Lifshitz 1959); hence, upper limit of the the integral over ξ is not the dimension of the body, L , but a fraction of it. The fraction itself is Reynolds number dependent – decreases with Reynolds number. Thus we expect that for large Reynolds number the t_* in reality is larger than the one obtained in Eq. (10). There is a second, crucial, implicit, assumption of scale invariance in deriving Eq. (10): the shape of the body does not change as the body erodes. This assumption is used in two places, once while assuming that the constant C does not depend on time and a second time while assuming that there is only one, time-dependent, length-scale L that determines the time-dependent volume. In other words, the body erodes in a self-similar manner. This may not be true at the initial stages of erosion – erosion at initial times may depend on the initial shape of the body – hence, the power-law dependence of volume on time may not be observed in early stages of erosion. Finally, note that while arriving at Eq. (7) we have assumed that ξ and η can be integrated independent of each other; this assumption can be relaxed to obtain essentially the same result.

The equations 9 and 10 are essentially a reworking of the results elucidated by Ristroph et al. (2012) and Moore et al. (2013), who instead of writing an equation for evolution of volume wrote one for the surface area which was confirmed by their experiments.

2.3. Direct numerical simulation

We study erosion by direct numerical simulation. This poses a difficult problem because we have to be able to solve the equations of the flow with an irregular boundary which itself evolves with time. Most Navier–Stokes solvers are unable to deal with such a problem. We choose to use the Lattice Boltzmann Method (LBM).

The Lattice Boltzmann Method, which is a descendant of the lattice gas algorithm, is used quite commonly in fluid mechanics. Hence, we do not give a detailed description of the algorithm here. It is described in great detail in several reviews (Chen & Doolen 1998; Benzi et al. 1992) and books (Sukop & Thorne 2007; Succi 2018). However, as its use in astrophysics is not very common, we do provide a short description in Appendix A. We follow Jäger et al. (2017) to implement erosion in our code, see section A.1 for further detail.

Here, it is sufficient to mention a few important aspects of our simulations. At the start of the simulation, grid points are classified as one of the three types: solid, fluid, and interface. In contrast to the theoretical framework presented in section 2.2 we do implement a threshold value for the solid stress. If the fluid stress exceeds this threshold value, an interface point loses mass following the empirical law of erosion, Eq. (1). Once the loss of mass exceeds a certain fixed value, m_0 , an interface point is changed to a fluid point and its erstwhile solid neighbors turn into interface. This introduces a new dimensionless parameter $m_0/(\rho_\bullet L^3)$. In reality, erosion is not a continuous process in time – it happens through sudden erosion of macroscopic dust grains. The parameter m_0 corresponds to the mass of such dust grains.

We benchmark our code, without the implementation of erosion, against standard test cases.

3. RESULTS

We first study the case of erosion of a solid sphere followed by that of a solid cube. Here, we present the results of the simulation of erosion of an irregular object we call the *snowman* which is made by merging two spheres – one smaller than the other, Fig. (2). We do this for two important reasons: first, as our principal motivation is erosion of planetesimals we consider a shape close to one that is expected to be typical of planetesimals; second, we expect that the departure from the theory, if any, is larger for such irregular-shaped objects.

3.1. Universal erosion

In Fig. (2) we show three different stages of erosion for a snowman with its axis oriented along the flow (symmetric snowman) and with an angle with the flow (asymmetric snowman) for $Re = 800$. In reality, the

eroding body is expected to rotate, which we ignore. In Fig. (3A) we show how the volume ($V(t)/V(0)$) of the snowman, the sphere, and the cube changes as a function of time, for five different Reynolds numbers: $Re = 100, 200, 400, 500$, and 800 . Remarkably, erosion for all these solids, irrespective of the Reynolds number, follows the same *universal law at intermediate times*. There is departure from this law at early times, particularly so for the cube, because erosion at early times is not universal but depends on the shape of the eroding object. In Fig. (3B), we plot the volume as a function of $1 - t/t_*$ in log-log scale. The theoretical expression, Eq. (8), shown as a black dashed line, is a very good approximation to our numerical results, except at late times. We do expect this departure at late times because when the solid becomes small the theory no longer applies.

Does the self-similar evolution of volume imply that eroding bodies, irrespective of their initial shape, reduces to the same shape? We find that this is not the case. In the last column of Fig. (2) we plot the shape of the eroded object for the three different initial shapes; the sphere, the symmetric snowman, and the asymmetric-snowman for $t/t_* \approx 0.5$ – a time at which the self-similar evolution holds. The three shapes are quite different from each other. Even at very late times, $t/t_* \approx 0.8$, shown in Fig. (5), the three different initial shapes do not become similar to each other.

Next, in Fig. (4) we plot the time scale t_* as a function of Re for different shapes. The black dashed lines shows the expected dependence $t_* \sim \sqrt{Re}$ – clearly they do not agree. For moderate Re we find, $t_* \sim Re^{0.8}$, shown as a red dashed line. This disagreement is due to several reasons. First, note that for any shape t_* is a non-monotonic function of Re . This is because beyond a critical Re the boundary layer separates (see, e.g., Landau & Lifshitz 1959, section 40). This implies that the upper limit of the integral in Eq. (7) over ξ is no longer L but smaller. This suggest that the erosion time should increase (as rate of mass loss decreases) but this is not the case in practice. Instead, the separation of boundary layer is accompanied by appearance of vortices behind the solid, we show several such examples in Fig. (2). These vortices are very efficient at eroding the solid thereby decreasing the erosion time by a large amount. But they are not accounted for in the theory we have described. Second, our numerical estimate of the erosion time, t_* is not very accurate. We estimate it by recording the time the solid disappears but the theory no longer applies as the solid becomes too small.

To summarize, our simulations show that the law of erosion given in Eq. (9) holds, at intermediate times,

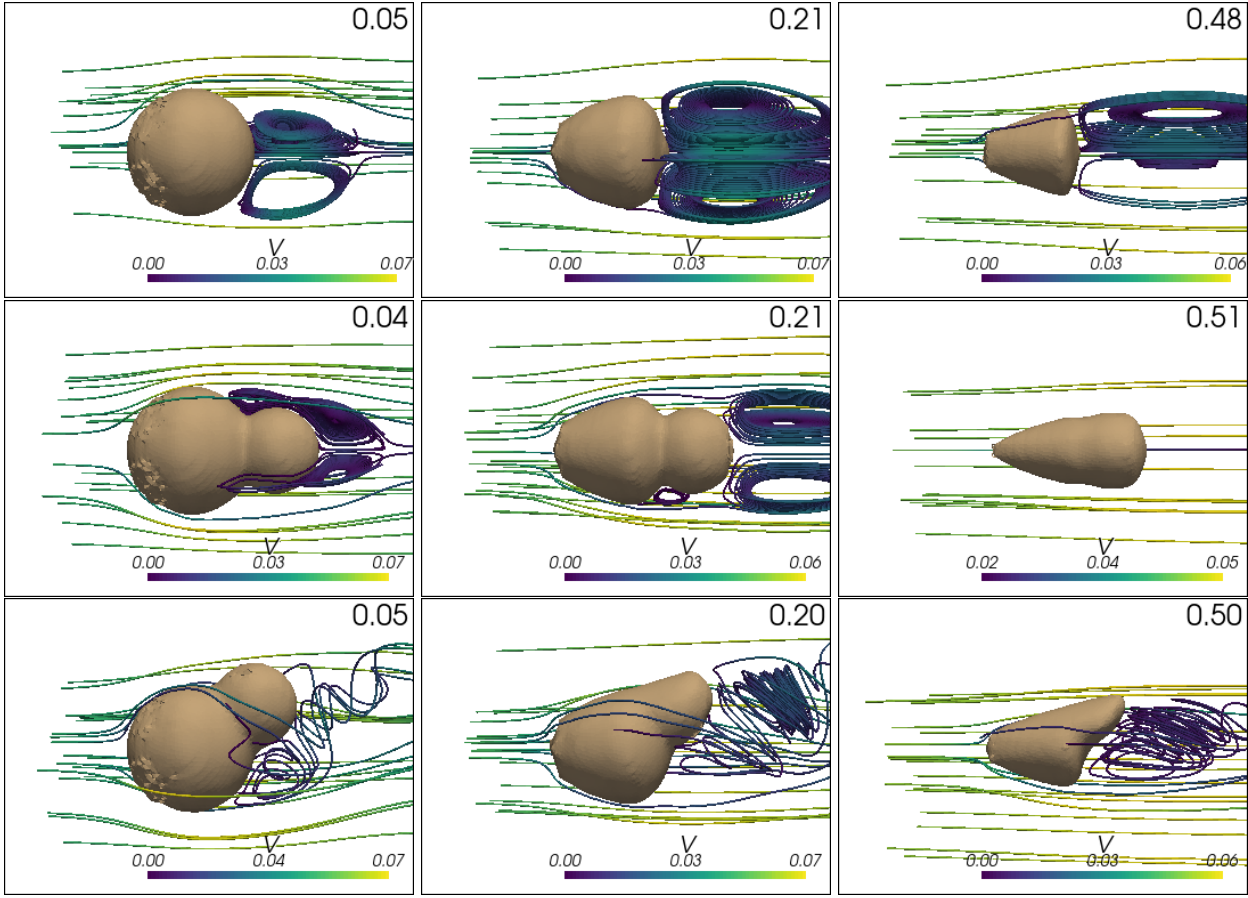


Figure 2. Erosion of sphere and *snowman* at $\text{Re} = 800$: the shape and topography of the sphere and the *snowman* as a function of time. We also plot some of the streamlines of the flow around the eroding body. Time in units of t_* is shown at the top right corner. Top row: the sphere. Middle row: the *symmetric snowman*, where the axis of the snowman is along the direction of the flow. In the bottom row, we plot the *asymmetric snowman*, where the axis of the snowman makes an angle with the flow. The blue streamlines show the vortices. The location and strength of these vortices depend on the shape of the snowman and its direction relative to the flow. These vortices make a significant contribution to erosion but they are not part of the theoretical framework. The color bar shows magnitude of velocity measured in units of sound speed. The simulations are performed using Lattice Boltzmann Method with a resolution of $120 \times 60 \times 60$ grid points.

for all the Reynolds numbers and the shapes we have studied suggesting that (9) is a universal law of erosion. But the dependence of t_* on Re is more complicated than the simple expression: $t_* \sim \sqrt{\text{Re}}$.

3.2. Erosion of planetesimals

To understand the implication of our results for erosion of bodies in protoplanetary disks we need to estimate the dimensionless numbers for the disk. We choose a simple model for protoplanetary disks:

$$\Sigma \sim R^{-\gamma} \quad \text{and} \quad c_s \sim R^{-\beta}, \quad (11)$$

where R is the distance from the central star, Σ is the surface mass density and c_s is the speed of sound. For example, in the minimum mass solar Nebula model (Hayashi 1981; Armitage 2010) $\gamma = 3/2$. The vertical scale height, $h(R)$, of the disk is $h \equiv c_s/\Omega_K$ where

$\Omega_K \equiv \sqrt{GM_\odot/R^3}$ is the Keplerian velocity (M_\odot is the mass of the central star and G the gravitational constant); the density at the midplane is $\rho(R) \sim \Sigma/h$; the particle number density $n(R) = \rho(R)/m_p$, where m_p is the mass of proton, the mean-free-path, $\lambda(R) = 1/n\sigma$, where $\sigma \approx 2 \times 10^{-15} \text{cm}^2$ is the cross section of molecular collisions, and the Mach number of the disk is $\text{Ma}_d(R) \equiv v_K/c_s \sim R/h$. A planetesimal is typically in an orbit around the central star with Keplerian speed $v_K = \sqrt{GM_\odot/R}$. The gas also rotates around the central star with a velocity close to but not equal to the Keplerian velocity. The difference in velocity is seen as a headwind by the planetesimal (Armitage 2010). The boulder in section 2.2 corresponds to a planetesimal and the velocity of this headwind corresponds to U . For a planetesimal on an eccentric orbit, the headwind is not a constant but depends on position of the planetesimal

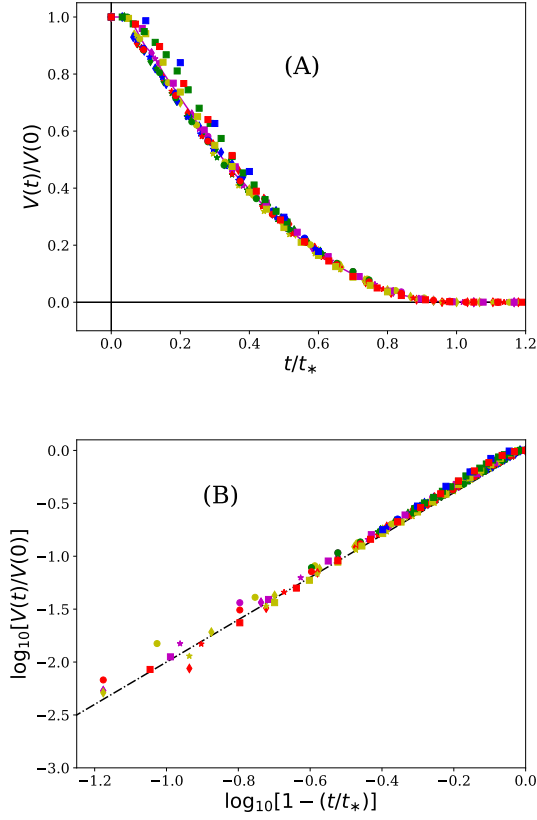


Figure 3. (A) Volume (normalized by the initial volume) of the solids as a function of time (normalized by t_*) for all our runs. The colors label Reynolds number: 100 (magenta), 200 (yellow), 400 (green), 500 (blue), 800 (red). The symbols label the shapes: \diamond (snowman with axis along the flow, symmetric snowman), $*$ (snowman with axis not long the flow, asymmetric snowman), \bullet (sphere) and \square (cube). (B) The same plot in log-log scale with the abscissa changed to, $1 - t/t_*$. The black dashed line has a slope of 2.

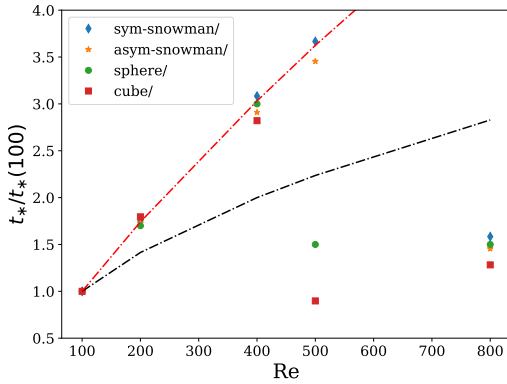


Figure 4. Value of t_* from our simulations as a function of the Reynolds number. The black dashed lines is \sqrt{Re} and the red dashed line is $Re^{0.8}$.

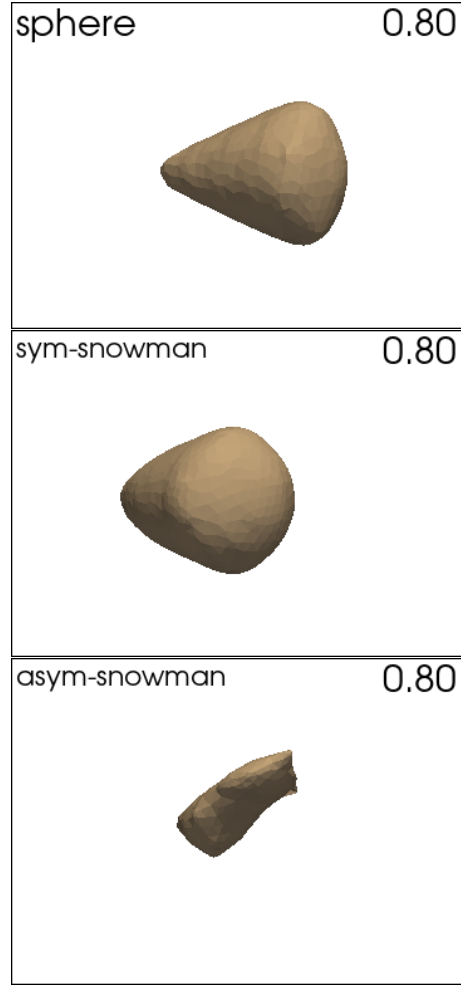


Figure 5. The shape of the eroded body at late times $t/t_* \approx 0.8$. The flow, which is not shown here, is from left to right.

and the details of its orbit. We consider an orbit with zero inclination. At the position where the cosine of its true anomaly is zero, the headwind is given by (Adachi et al. 1976)

$$U = v_K \sqrt{e^2 + \eta^2}, \quad (12)$$

where $\eta \propto c_s^2/v_K^2$, is a dimensionless number that can be as small as 10^{-3} depending on the position in the disk. Hence, we obtain $T\Omega_K = T_K(2\pi L/R)(1/\sqrt{e^2 + \eta^2})$. The Reynolds number of a solid of size L in a orbit at a distance R from the central star can be estimated to be (see, e.g., Mitra et al. 2013)

$$\begin{aligned} Re &= Ma \frac{L}{\lambda} \approx \sqrt{e^2 + \eta^2} Ma_d \frac{L}{\lambda} \\ &\approx \sqrt{e^2 + \eta^2} \left(\frac{R}{h}\right) \left(\frac{L}{\lambda}\right). \end{aligned} \quad (13)$$

The Mach number of the headwind is related to the disk Mach number, $Ma_d \equiv v_K/c_s \approx R/h$, where h is the

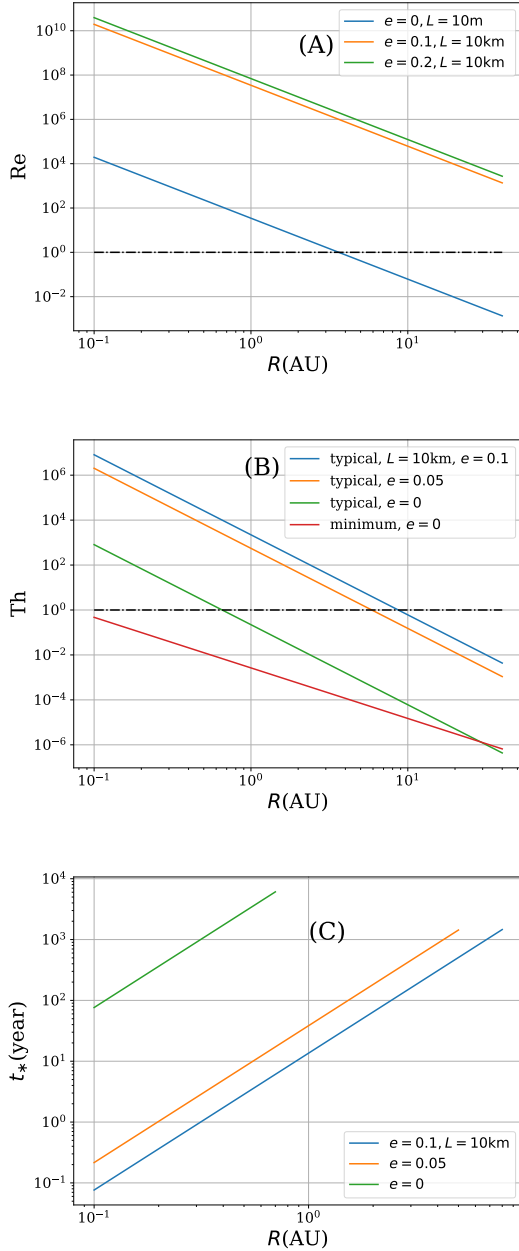


Figure 6. We consider a 10 km sized body at a distance R from the central star with one solar mass. The exponents for the surface density and sound speed, see Eq. (11), are $\gamma = 3/2$ and $\beta = 3/8$. We have also chosen $\Lambda = 10$. (A) The Reynolds number as a function of R (in astronomical units) and (B) The dimensionless threshold, Th , as a function of R (in astronomical units). The threshold stress $\tau_s = 0.0011$ Pa. (C) The time it takes for a 10km sized planetesimal to erode away as a function of the semi-major axis of its orbit calculated using Eq. (10). We use $\kappa_{er} \approx 150\text{m}^{-1}\text{s}$ and $\rho_\bullet = 536\text{kgm}^{-3}$ (Pätzold et al. 2019). For each of the three cases we plot, from (B) we calculate the maximum R below which $Th > 1$, i.e. erosion occurs. For planetesimals on orbits whose semi-major axis is greater than this maximum R Eq. (10) is no longer valid because such planetesimals do not erode.

vertical scale height of the disk at a radius R from the central star, $Ma = \sqrt{e^2 + \eta^2} Ma_d$. Substituting these expressions in Eq. (5), we find how the dimensionless parameters depend on the radial coordinate of the disk:

$$Re \sim R^{2\beta-\gamma-2} \quad (14a)$$

$$Er \sim R^{-1/2} \quad (14b)$$

$$Th_{\min} \sim R^{\gamma/2-1} \quad Th_{\text{typ}} \sim R^{\beta/2-\gamma-9/4} \quad (14c)$$

To give a specific example, we now consider a body with $L = 10$ km at a distance R from the central star with one solar mass. The exponents for the surface density and sound speed, see Eq. (11), are $\gamma = 3/2$ and $\beta = 3/8$ – a minimum mass Solar Nebula model for a razor-thin disk. In Fig. (6A), we plot Re as a function of R . Estimation of the other two dimensionless numbers Er and Th is less certain.

Let us first consider the dimensionless threshold, Th . Experiments in laboratory (White et al. 1987; Paraskov et al. 2006) have tried to estimate the threshold stress necessary to lift dust grains from the surface of a pile of grains. Unlike these experiments, erosion of a boulder in a protoplanetary disk does not depend on gravity. Experiments in microgravity (Musiolik et al. 2018; Demirci et al. 2019; Kruss et al. 2020; Demirci et al. 2020) have tried to approach lower and lower gravity and ambient pressure to get as close to the condition of protoplanetary disks as possible. The last of these (Demirci et al. 2020) measured the critical shear stress of a pile of glass beads in a parabolic flight campaign. The critical shear stress depends on the size of the glass beads and ambient pressure (Demirci et al. 2020, figure 5). They conclude that “..cohesion is really low. At zero gravity, the shear stress required to initiate erosion is only 0.0011 Pa”, i.e., $\tau_s \approx 0.0011$ Pa! Substituting in Eq. (5) we calculate both the typical value of Th and its minimum value. In Fig. (6B), we plot the typical value of Th for orbits with three different eccentricities, $e = 0.1, 0.05$, and zero (circular orbit). For the first one, the dimensionless threshold remains greater than unity for $R \lesssim 9\text{au}$. For the second one, $e = 0.05$, the dimensionless threshold remains greater than unity for $R \lesssim 8\text{au}$. For orbits of even higher eccentricities erosion remains important for even larger values of R . For an orbit of zero eccentricity the typical value of Th remains greater than unity for $R \lesssim 0.6\text{au}$. If instead of the typical value of Th we consider its minimum value then the dimensionless threshold for a circular orbit is less than unity everywhere. We conclude that typically, erosion occurs for eccentric orbits, even with eccentricity as small as 0.05 in the inner disk. Erosion happens even for boulders

in perfectly circular orbits if they are close enough to the central star. This result is different from our earlier work (Schaffer et al. 2020) because of two reasons: (a) In the light of recent experimental results (Demirci et al. 2020) we consider a lower value of τ_s . (b) We consider the typical fluid stress not the minimum value as we had done before.

There is even less experimental data to estimate the erosion number Er . As in our earlier work (Schaffer et al. 2020), following Demirci et al. (2019), we assume a value of $\kappa_{er} \approx 150(\text{s/m})$. In Fig. (6C) we plot the time it takes for body to erode away, t_* from Eq. (10), with $L = 10\text{km}$, and $\rho_\bullet = 536\text{kgm}^{-3}$ (Pätzold et al. 2019). We first consider t_* (blue line) for an orbit with eccentricity $e = 0.1$. From Fig. (6B), we know that for such an orbit erosion happens if $R \lesssim 9\text{au}$. Hence, we plot t_* for $R \lesssim 9\text{au}$. For orbits with R less than this limit t_* ranges from less than a year to about 200 years, extremely short times in astronomical time scales. For orbits with R larger than this value erosion has no effect. For an orbit with eccentricity $e = 0.05$, t_* [orange line in Fig. (6C)] ranges from less than a year to about 300 years, only if $R \lesssim 8\text{au}$. Even for a circular orbit (green line) t_* ranges from about 100 years to little less than ten thousand years, only if $R \lesssim 0.6\text{au}$. Hence, we conclude that planetesimals in eccentric orbits, of even very small eccentricity, rapidly (in about hundred years) erodes away if the semi-major axis of their orbit lies in the inner disk (less than about 10 au). Even planetesimals in circular orbits erode away in about ten thousand years if the semi-major axis of their orbits are closer than 0.9au.

4. CONCLUSION

In a recent paper Rozner et al. (2020), have argued that under erosion $dL/dt \sim 1/L$. This is different from the law, Eq. (9), we report. Our result is supported by theory (Ristroph et al. 2012; Moore et al. 2013), our numerical simulations and experiments (Ristroph et al. 2012). Furthermore, unlike us, Rozner et al. (2020) do not take into account the dynamics of the problem, i.e., the fact that the fluid stress eroding the body changes as the body erodes. However, they also reach the same qualitative conclusion that erosion is rapid.

Let us repeat that we find, contrary to our earlier work (Schaffer et al. 2020), that erosion happens even for boulders in perfectly circular orbits if they are close enough to the central star. This is so because of two reasons: (a) in the light of recent experimental results (Demirci et al. 2020), we consider a lower value of τ_s and (b) we consider the typical fluid stress not the minimum value as we had done before.

4.1. How robust are our results?

The law of erosion, Eq. (9), is derived under several simplifying assumptions. Our simulations, which are not limited by those assumptions, for the first time, show its universal nature – the law holds for all the shapes and the Reynolds numbers we consider, irrespective of whether the laminar boundary layer has become unstable or not. But the expression for the time it takes for the body to erode away, t_* , does not follow the simple theory. At small Reynolds numbers, it is typically larger than the theoretical prediction, at large Reynolds numbers it is typically smaller. We estimate the Reynolds number of a 10km sized boulder to be 10^4 or larger, Fig. (6). Hence, we expect that in reality the time it takes for a 10km sized planetesimal to erode away is shorter than the t_* we estimate in Fig. (6C).

The estimate of the dimensionless threshold (Th) is less certain. Our estimate for the threshold stress, τ_s , may be a gross underestimate if the planetesimal contains snow. Hence, we expect effects of erosion to be small beyond the snow line. Furthermore, different layers on the planetesimal may have different threshold stress; the inner layers may be more strongly held due to sintering. Once exposed, it may take longer to erode them. It is straightforward to add such effects to our simulations but is futile as we do not know quantitatively the effects of sintering in planetesimals. Note that even if τ_s increases by a factor of 10 or 100, erosion will still occur although at shorter distance from the central star or in orbits with higher eccentricity.

The estimate of the erosion number is also uncertain because of the uncertainty regarding κ_{er} . We know of only one experiment (Demirci et al. 2020) from which we estimate κ_{er} . If this number is smaller by a factor of 10, t_* increases by a factor of 10. Even then erosion is rapid in astronomical time scales.

Naturally, erosion is also accompanied by deposition. Deposition also happens with a threshold stress but this threshold is typically lower than the erosion threshold (Salles et al. 1993). In the range between these two thresholds the body neither grows nor decays. In this paper we have ignored deposition. It is possible that planetesimals close to the central star erode, while the material that is eroded is deposited on the planetesimals further away such that their growth rate actually increases.

Finally, note that in a protoplanetary disk the gas flow is turbulent, whereas in our model (both theoretical and numerical) we have assumed the incoming flow to be laminar. Very little is known about drag, lift, or wall stress of bodies in flows that are already turbulent. We can speculate that in such cases we will have an even

thinner and highly fluctuating boundary layer. This we leave for the future.

4.2. Application to objects in the asteroid belt

How do we reconcile our results with the fact that the asteroid belt of the solar system has many objects with sizes ranging from about a kilometer to hundreds of kilometers in eccentric orbits? The asteroid belt lies between two and three au. As a specific example, consider the minor planet Vesta, which is about 500 km in size in an orbit with eccentricity about 0.09 and a semimajor axis of about 2.3au. According to our theory such asteroids could not form where they are at present by mere aggregation because they would have eroded away as soon as they formed. This gives rise to several possibilities. One, Vesta was formed originally on a circular orbit but developed the small eccentricity it now has at a later stage when the gas in the disk had disappeared. Two, Vesta originally formed further away in the disk and had migrated inward at a later stage. Three – the most interesting one – these asteroids originally formed, by gravitational collapse, as much bigger bodies and have eroded away to their present size in a time scale of about a megayear – the approximate lifetime of the disk. We discuss this possibility next.

Consider the possibility that the gravitational collapse creates a body of approximate size of 10^3 km. To apply our results to such a body we must also include the gravitational pull by the body itself. Figure 7 in the article by (Demirci et al. 2020) suggests that the threshold stress increases linearly with gravity with a proportionality constant $\alpha \approx 7 \times 10^{-2}$ in units of kilograms divided by meter squared. Hence, the threshold stress of a 10^3 km body is $\tau_s \approx 0.001\text{Pa} + \alpha g$ where g is the gravitational acceleration on the surface of the asteroid given by: $g = g_\oplus R_\oplus / R$ where $g_\oplus \approx 9.8\text{ms}^{-2}$ is the acceleration on the surface of Earth and $R_\oplus \approx 6400$ km is the radius of Earth. For a body of size approximately 10^3 km we obtain $\tau_s \approx 0.1$ Pa. For this case, our calculations show that the dimensionless threshold is greater than unity for an orbit with $e = 0.1$ up to a distance of about 2 au. We further find that such a body will

erode away in about 10^5 years. However, the value of the constant κ_{er} , which determines the rate of erosion, is not known accurately and also, like τ_s , should depend on gravity. We have no experimental data on this. Clearly, larger gravity implies that κ_{er} is smaller. If we consider a much smaller $\kappa_{\text{er}} \approx 8\text{m}^{-1}\text{s}$ we find that $t_* \approx 8 \times 10^6$ years. In other words, if we consider the lifetime of the disk to be about 10^6 years a 10^3 km body at a distance of about 2 au that has formed by gravitational collapse on a orbit with eccentricity of 0.1 will erode away *partially but not completely*. After being eroded for 10^6 years the size of the body is going to be approximately 300 km. Of course, none of the specific numbers in this paragraph are supposed to be precise. Thus, we illustrate that our theory is consistent with the recently suggested hypothesis (Klahr & Schreiber 2020, 2021) that the planetesimals form by gravitational collapse to bodies of about 100 km in size or larger.

ACKNOWLEDGEMENTS

The code to plot Fig. (2) was written by Aritra Bhakat. All figures in this paper are plotted using the free software matplotlib (Hunter 2007). DM thanks Srikanth Toppaladoddi, Alessandro Morbideli, and John Wettlaufer for stimulating discussions. We thank Prasad Perlekar for helping us write the lattice Boltzmann code.

This work is partially funded by the “Bottle-necks for particle growth in turbulent aerosols” grant from the Knut and Alice Wallenberg Foundation (2014.0048). In addition, A.J. acknowledges funding from the Swedish Research Council (grant 2014-5775), the Knut and Alice Wallenberg Foundation (grants 2012.0150, 2014.0017) and the European Research Council (ERC Consolidator Grant 724687-PLANETESYS) for research support. B.M. acknowledges funding from the Swedish Research Councils (grant 2017-3865) D.M. acknowledges funding from the Swedish Research Council (638-2013-9243, 2016-05225). The simulations were performed on resources provided by the Swedish National Infrastructure for Computing (SNIC) at PDC center for High Performance Computing.

APPENDIX

A. LATTICE BOLTZMANN METHOD

Instead of solving the Navier–Stokes equation the Lattice Boltzmann Method solves the Boltzmann equation on a Cartesian lattice. Recall, that the Boltzmann equation is an equation of evolution of probability density function, $f(\mathbf{x}, \mathbf{v}, t)$, of molecules in *phase space*, where \mathbf{x} is the physical coordinates and \mathbf{v} is the velocity coordinates of phase space (see, e.g., Lifshitz & Pitaevskii 1993). A hydrodynamic description of the system emerges on averaging over the

phase-space, i.e, the hydrodynamic density,

$$\rho(\mathbf{x}, t) \equiv \int f(\mathbf{x}, \mathbf{v}, t) d^d v, \quad (\text{A1})$$

and the hydrodynamic momentum,

$$\rho \mathbf{u}(\mathbf{x}, t) \equiv \int \mathbf{v} f(\mathbf{x}, \mathbf{v}, t) d^d v, \quad (\text{A2})$$

The hydrodynamic pressure and the stress tensor emerges as respectively the isotropic and non-isotropic part of

$$\sigma_{\alpha\beta} \equiv \int c_\alpha c_\beta f(\mathbf{x}, \mathbf{v}, t) d^d v, \quad (\text{A3})$$

where the Greek indices denote Cartesian components and $c_\alpha \equiv \mathbf{v} - \mathbf{u}$. Thus, once we have numerically solved the Boltzmann equation it is straightforward to obtain the hydrodynamic variables, which are guaranteed to satisfy the Navier-Stokes equation. The proof of this last statement is through the Chapman–Enskog expansion. The proof becomes significantly simpler if the collision integral on the right hand side of the Boltzmann equation is replaced by its Bhatnagar–Gross–Krook (BGK) approximation, which postulates that the only effect of collision is that at every grid point in physical space f relaxes to its equilibrium value – a Maxwellian distribution – with a single characteristic time-scale τ . Within the BGK approximation, the kinematic viscosity of the fluid is

$$\nu = (\tau - 1/2) \quad (\text{A4})$$

To solve the Boltzmann equation numerically we need to discretize the physical space but more importantly also the velocity space. The velocity space is discretized into 27 discrete lattice vectors, this is known as the D3Q27 model of the LBM. These lattice vectors are plotted in Fig. (7). Once we solve for f by solving the discrete Boltzmann equation it is straightforward to calculate the velocity, density, and the stress tensors from f by replacing the integral in equations A1, A2, and A3 by a sum over the twenty seven discrete values of velocity.

A major advantage of this method is the way it deals with boundary conditions. We use a technique called *bounce back* to model no-slip boundary conditions, as we show in Fig. (8). The shaded part of the figure is the solid and the grid points there are classified as solid grid points. The physical boundary is imagined halfway between the grid points, the boundary between the shaded and the unshaded region. The $\mathbf{v} \cdot \nabla f$ term in the Boltzmann equation denotes streaming of the component of f along a particular lattice vector \mathbf{q} by the velocity along that direction. In Fig. (8a) show a grid point with three lattice vectors.

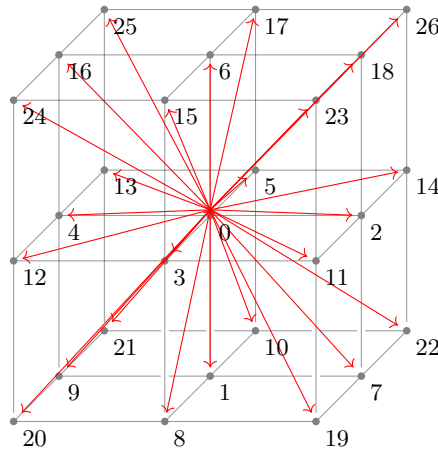


Figure 7. 3D visualization of the twenty seven discrete lattice vectors (one of them is zero) used to discretize the distribution function f in lattice Boltzmann algorithm D3Q27.

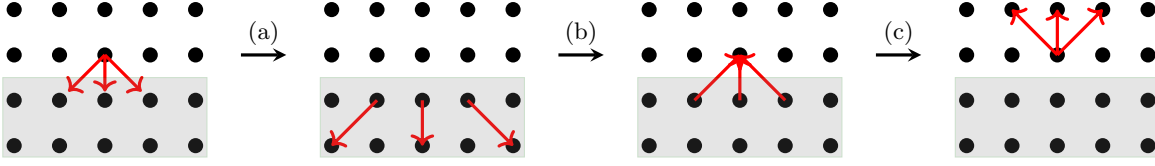


Figure 8. Bounce back sequence. (a) is the streaming step. (b) is the bounce back boundary condition. (c) is streaming step again. Gray area represents the solid domain while the white represents the fluid domain.

A.1. Implementation of erosion

Our numerical scheme follows Jäger et al. (2017). Let the deviatoric stress tensor be

$$\sigma_{\alpha\beta} \equiv \mu (\partial_{\alpha} u_{\beta} + \partial_{\beta} u_{\alpha}). \quad (\text{A5})$$

The shear force at an infinitesimal surface element dS with unit normal \hat{n} is given by $F_{\alpha} = \sigma_{\alpha\beta} n_{\beta}$. The magnitude of the tangential component of this force is the wall shear stress

$$\tau_{\text{f}} = | \mathbf{F} - \hat{n} \cdot \mathbf{F} | \quad (\text{A6})$$

In the lattice Boltzmann method this is calculated as

$$\sigma_{\alpha\beta} = \left(1 - \frac{1}{2\tau} \right) \sum_i f_i^{\text{neq}}(\mathbf{c}_i)^{\alpha} (\mathbf{c}_i)^{\beta}, \quad (\text{A7})$$

where $f_i^{\text{neq}} = f_i - f_i^{\text{eq}}$ is the nonequilibrium part of the distribution function (Jäger et al. 2017) and i runs over the lattice vectors – 27 in the D3Q27 model.

REFERENCES

- Adachi, I., Hayashi, C., & Nakazawa, K. 1976, *Progress of Theoretical Physics*, 56, 1756
- Armitage, P. J. 2010, *Astrophysics of Planet Formation* (Cambridge, UK: Cambridge University Press)
- Barge, P., & Sommeria, J. 1995, *Astronomy and Astrophysics*, 295, L1
- Benzi, R., Succi, S., & Vergassola, M. 1992, *Physics Reports*, 222, 145
- Blum, J., & Wurm, G. 2008, *ARA&A*, 46, 21, doi: [10.1146/annurev.astro.46.060407.145152](https://doi.org/10.1146/annurev.astro.46.060407.145152)
- Chen, S., & Doolen, G. D. 1998, *Annual review of fluid mechanics*, 30, 329
- Demirci, T., Kruss, M., Teiser, J., et al. 2019, *Monthly Notices of the Royal Astronomical Society*, 484, 2779
- Demirci, T., Schneider, N., Steinpilz, T., et al. 2020, *Monthly Notices of the Royal Astronomical Society*, 493, 5456
- Hayashi, C. 1981, in *Fundamental Problems in the Theory of Stellar Evolution*, ed. D. Sugimoto, D. Q. Lamb, & D. N. Schramm, Vol. 93 (Dordrecht, D. Reidel Publishing Co.), 113–126
- Hunter, J. D. 2007, *Computing in Science & Engineering*, 9, 90, doi: [10.1109/MCSE.2007.55](https://doi.org/10.1109/MCSE.2007.55)
- Jäger, R., Mendoza, M., & Herrmann, H. J. 2017, *Physical Review E*, 95, 013110
- Johansen, A., Blum, J., Tanaka, H., et al. 2014, in *Protostar and Planets VI*, ed. H. Beuther, R. S. Klessen, C. P. Dullemond, & T. Henning (University of Arizona Press, Tucson), 547–570
- Johansen, A., Oishi, J. S., Mac Low, M.-M., et al. 2007, *Nature*, 448, 1022
- Johansen, A., Youdin, A., & Klahr, H. 2009, *The Astrophysical Journal*, 697, 1269
- Klahr, H., & Bodenheimer, P. 2006, *The Astrophysical Journal*, 639, 432
- Klahr, H., & Schreiber, A. 2020, *The Astrophysical Journal*, 901, 54
- . 2021, *The Astrophysical Journal*, 911, 9
- Kruss, M., Musiolik, G., Demirci, T., Wurm, G., & Teiser, J. 2020, *Icarus*, 337, 113438
- Landau, L., & Lifshitz, E. 1959, *Course of Theoretical Physics, Vol. 6, Fluid mechanics* (Oxford, England: Pergamon Press Ltd.)
- Lifshitz, E., & Pitaevskii, L. 1993, *Course of Theoretical Physics, Vol. 10, Physical Kinetics* (Oxford, England: Pergamon Press Ltd.)

- Mac Huang, J., Moore, M. N. J., & Ristroph, L. 2015, *Journal of Fluid Mechanics*, 765, R3
- Mitra, D., Wettlaufer, J. S., & Brandenburg, A. 2013, *The Astrophysical Journal*, 773, 120
- Moore, M. N., Ristroph, L., Childress, S., Zhang, J., & Shelley, M. J. 2013, *Physics of Fluids*, 25, 116602
- Musiolik, G., Kruss, M., Demirci, T., et al. 2018, *Icarus*, 306, 25
- Paraskov, G. B., Wurm, G., & Krauss, O. 2006, *The Astrophysical Journal*, 648, 1219
- Pätzold, M., Andert, T. P., Hahn, M., et al. 2019, *Monthly Notices of the Royal Astronomical Society*, 483, 2337
- Ristroph, L., Moore, M. N., Childress, S., Shelley, M. J., & Zhang, J. 2012, *Proceedings of the National Academy of Sciences*, 109, 19606
- Rozner, M., Grishin, E., & Perets, H. B. 2020, *Monthly Notices of the Royal Astronomical Society*, 496, 4827
- Salles, J., Thovert, J., & Adler, P. 1993, *Chemical Engineering Science*, 48, 2839
- Schaffer, N., Johansen, A., Cedenblad, L., Mehling, B., & Mitra, D. 2020, *Astronomy & Astrophysics*, 639, A39, doi: [10.1051/0004-6361/201935763](https://doi.org/10.1051/0004-6361/201935763)
- Shields, I. 1936, PhD thesis, University of Berlin. <https://authors.library.caltech.edu/25992/1/Sheilds.pdf>
- Subhasish, D. 2014, *Fluvial Hydrodynamics* (Springer-Verlag Berlin Heidelberg), doi: [10.1007/978-3-642-19062-9](https://doi.org/10.1007/978-3-642-19062-9)
- Succi, S. 2018, *The lattice Boltzmann equation: for complex states of flowing matter* (Oxford: Oxford University Press)
- Sukop, M. C., & Thorne, T. D. J. 2007, *Lattice Boltzmann Modeling* (Springer-Verlag Berlin Heidelberg)
- Wettlaufer, J. S. 2010, *ApJ*, 719, 540, doi: [10.1088/0004-637X/719/1/540](https://doi.org/10.1088/0004-637X/719/1/540)
- White, B., Greeley, R., Leach, R., & Iversen, J. 1987, in *25th AIAA Aerospace Sciences Meeting (AIAA)*, 621, doi: [10.2514/6.1987-621](https://doi.org/10.2514/6.1987-621)
- Wilkinson, M., Mehlig, B., & Uski, V. 2008, *The Astrophysical Journal Supplement Series*, 176, 484
- Youdin, A. 2010, in *EAS Publications Series*, Vol. 41, *PHYSICS AND ASTROPHYSICS OF PLANETARY SYSTEMS*, ed. . A.-M. L. T. Montmerle, D. Ehrenreich (EDP Sciences), 187–207
- Youdin, A. N., & Goodman, J. 2005, *The Astrophysical Journal*, 620, 459
- Zsom, A., Ormel, C., Dullemond, C., & Henning, T. 2011, *A&A*, 534, A73